This study investigates residual circulation in the Peral River estuary using the Lagrangian residual velocity. It evaluated the contribution of each component of the Lagranigian residual velocity and in particular analyzed the four components of turbulent mean component. The results are interesting. I have few concerns and hope they can be clarified before publication of this manuscript in OS.

Response: We extend our sincere appreciation for your dedicated and insightful review of our manuscript. Your meticulous examination and thoughtful comments have been invaluable in refining and strengthening our work.

1. The decomposition of Lagrangian residual velocity

The decomposition method basically is to use the Coriolis term in momentum balance in which each term is divided by the Coriolis parameter. Because the velocity in the Coriolis term is cross correspondence, i.e. u is in the momentum balance of v, and v is in the momentum balance of u. Thus, the physical meaning of each velocity component is hard to explain. For example, the baroclinic pressure gradient component of u is related to density gradient in y direction. That doesn't make sense. Furthermore, if there is no Coriolis force, how do you decompose the velocity?

Response: Thank you for your professional comments on this research and also thanks for providing this opportunity to explain our work.

The decomposition method has physical meaning when the Coriolis force is important. The Pearl River Estuary (PRE) features a relatively wide expanse, measuring 20–60 km in width in the middle and lower regions, away from the river discharge input nodes, and extending over a length of 70 km. The Rossby number is approximately 0.2

in the Pearl River Estuary (PRE), similar to that calculated by Li et al. (2023), signifying the prominence of the Coriolis force in the region's dynamics. The baroclinic Rossby deformation radius is estimated to be approximately 12–16 km, a range similar to the findings of Pan et al. (2014), suggesting the necessity to account for the rotational effect of the Earth. Lai et al. (2018) highlighted that the influence of the Coriolis force in the PRE is substantial with its effect extending to the bottom layer when compared to vertical mixing, and baroclinic and barotropic momentum when analyzing the Eulerian average momentum equation. Chen et al. (2019) indicated that in the depth-integrated momentum balance prior to a storm in the PRE, local momentum balance primarily involves the pressure gradient force, the Coriolis force, and bottom stress. Synthesizing current and prior research, it becomes apparent that the Coriolis force is a predominant factor influencing the dynamics of the PRE. The aforementioned discussion accentuates the criticality and practicality of employing decomposition methods in such analytical contexts.

The physical dynamics within the Pearl River Estuary (PRE) can be elucidated as follows: the cross-estuary Lagrangian mean momentum equation is characterized by quasi-geostrophic balance, whereas the along-estuary Lagrangian mean momentum equation conforms to a blend of quasi-geostrophic and Ekman balances. That is because the cross-estuary Lagrangian Residual Velocity (LRV) is predominantly influenced by the interplay of barotropic and baroclinic pressure gradient components, alongside eddy viscosity components. Conversely, the along-estuary LRV is chiefly propelled by barotropic and baroclinic pressure gradient components. The aggregate of local

acceleration, horizontal nonlinear advection, and vertical nonlinear advection terms make a lesser and inverse contribution to the overall LRV. The input from the horizontal diffusion component is minimal, verging on negligible, as demonstrated in Fig. A1. Consequently, the Lagrangian mean momentum equations can be approximately simplified as follows:

$$-fv_L \approx -\underbrace{\langle g\frac{\partial \zeta}{\partial x}\rangle}_{1} - \underbrace{\langle \frac{g}{\rho_0}\left(D\int_\sigma^0 \frac{\partial \rho}{\partial x}d\sigma_1 + \frac{\partial D}{\partial x}\int_\sigma^0 \sigma_1 \frac{\partial \rho}{\partial \sigma_1}d\sigma_1\right)\rangle}_{2}, \quad \text{(A1)}$$

$$fu_L \approx \underbrace{-\langle g\frac{\partial \zeta}{\partial y}\rangle}_{1}\underbrace{-\langle \frac{g}{\rho_0}\left(D\int_\sigma^0 \frac{\partial \rho}{\partial y}d\sigma_1 + \frac{\partial D}{\partial y}\int_\sigma^0 \sigma_1 \frac{\partial \rho}{\partial \sigma_1}d\sigma_1\right)\rangle}_{2} + \underbrace{\langle \frac{1}{D^2}\frac{\partial}{\partial \sigma}\left(v_h\frac{\partial v}{\partial \sigma}\right)\rangle}_{3}, \quad \text{(A2)}$$

where The symbol <> represents the Lagrangian mean, the terms on the left-hand side of Eqs. (A1) and (A2) denote the Lagrangian mean Coriolis force. Conversely, the first and second terms on the right-hand side of these equations correspond to the Lagrangian mean barotropic and baroclinic pressure gradient forces, respectively. Furthermore, the third term on the right-hand side of Eq. (A2) represents the Lagrangian mean eddy viscosity term.

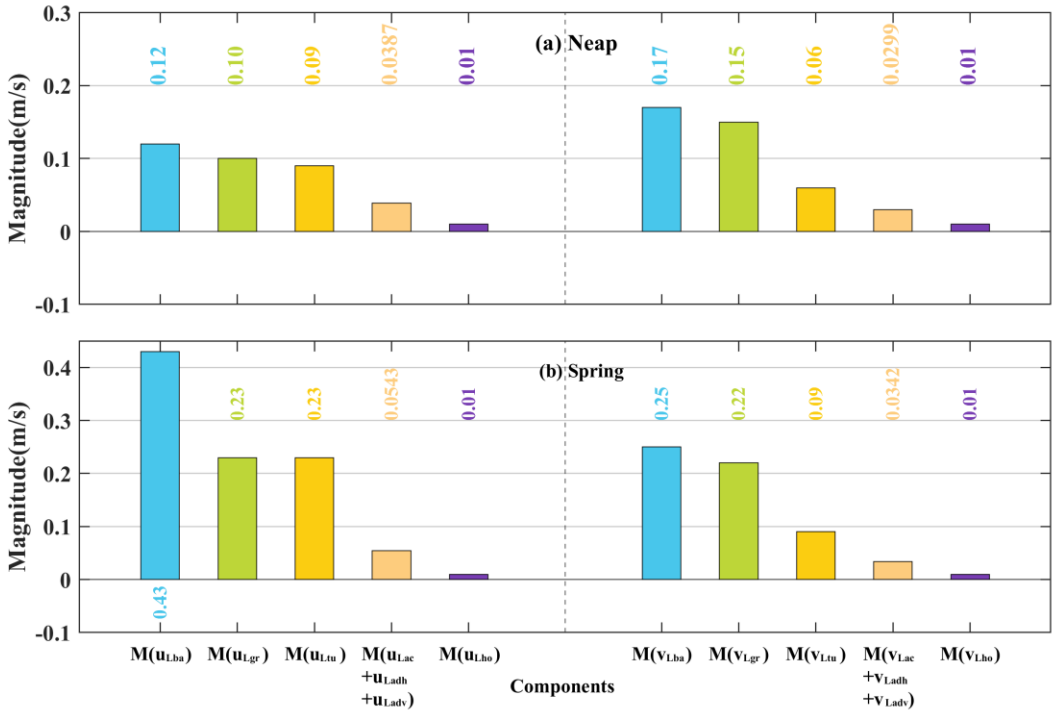

Figure A1 Bar charts for the magnitudes of individual components of u_L and v_L. The notation M(·) corresponds to the mean of absolute values for the components discussed in Section C. Specifically, M(u_{Lba}) quantifies the mean of the absolute values for the barotropic component, M(u_{Lgr}) for the baroclinic component, and M(u_{Ltu}) for the eddy viscosity component. Additionally, M(u_{Lac}+u_{Ladh}+u_{Ladv}) aggregates the mean of absolute values for the combined local acceleration, horizontal advection, and vertical advection components. M(u_{Lho}) calculates the mean of the absolute values for the horizontal diffusion component. Corresponding measurements for along-estuary components, namely M(v_{Lba}), M(v_{Lgr}), M(v_{Ltu}), M(v_{Lac}+v_{Ladh}+v_{Ladv}), and M(v_{Lho}), are analogously defined and follow a similar interpretative framework.

Analogous decomposition methodologies have been implemented in prior studies, notably in the research conducted by Wu et al. (2018). Their investigation delineated that a pivotal premise of Eq. (6) hinges on the assumption of a minimal Rossby number, thereby emphasizing the paramount importance of Coriolis forces within the framework

of Eulerian residual transport dynamics analysis. The equation for V_R (Wu et al., 2018) is as follows:

$$V_R = -\frac{1}{fH}\left\langle u_s \frac{\partial \eta}{\partial t}\right\rangle + \frac{\langle ADV\rangle}{fH} + \frac{g}{2fH}\frac{\partial\langle\eta^2\rangle}{\partial x} + \frac{g}{f}\frac{\partial\langle\eta\rangle}{\partial x} - \frac{\langle\tau_x^s\rangle}{\rho fH} + \frac{\langle\tau_x^b\rangle}{\rho fH} + \mathrm{Re}\ si, \qquad (6)$$

where V_R represents the north-south component of Eulerian residual transport, and the angle brackets denote the Eulerian mean. The first two terms on the right side of equation (6) represent local acceleration and the nonlinear advection components, respectively; the third and fourth terms correspond to the pressure gradient forcing; the fifth and sixth terms represent surface wind stress and bottom friction forcing, respectively; the seventh term encompasses other components.

The decomposition methodologies present distinct advantages for elucidating the dynamics of Lagrangian Residual Velocity (LRV) within generally or weakly nonlinear systems. This significance stems from the absence of comprehensive analytical solutions and definitive governing equations for LRV in generally nonlinear contexts, coupled with the constraints of analytical solutions in weakly nonlinear frameworks (Jiang and Feng, 2014; Cui et al., 2019; Chen et al., 2020).

In scenarios where the Coriolis force is negligible, the Lagrangian mean momentum equations remain applicable for primary momentum balance analysis. However, these equations are inadequate for the detailed dissection of each LRV component. Notably, in circumstances where the Coriolis effect is minimally impactful, the methodologies employed for LRV decomposition may demonstrate variability, contingent upon the dominant momentum balances. This underscores the necessity for expanded investigation in future scholarly endeavors.

The relative contents have been added to the revised manuscript (lines 697–715; lines 765–776): "*The Pearl River Estuary (PRE) features a relatively wide expanse, measuring 20–60 km in width in the middle and lower regions, away from the river discharge input nodes, and extending over a length of 70 km. The Rossby number is approximately 0.2 in the Pearl River Estuary (PRE), similar to that calculated by Li et al. (2023), signifying the prominence of the Coriolis force in the region's dynamics. The baroclinic Rossby deformation radius is estimated to be approximately 12–16 km, a range similar to the findings of Pan et al. (2014), suggesting the necessity to account for the rotational effect of the Earth. Lai et al. (2018) highlighted that the influence of the Coriolis force in the PRE is substantial with its effect extending to the bottom layer when compared to vertical mixing, and baroclinic and barotropic momentum when analyzing the Eulerian average momentum equation. Chen et al. (2019) indicated that in the depth-integrated momentum balance prior to a storm in the PRE, local momentum balance primarily involves the pressure gradient force, the Coriolis force, and bottom stress. Synthesizing current and prior research, it becomes apparent that the Coriolis force is a predominant factor influencing the dynamics of the PRE. This assertion is corroborated by Wu et al. (2018), who contend that the decomposition approach to Eulerian residual transport assumes particular significance in scenarios marked by a notable presence of Coriolis forces, as evidenced by a small Rossby number. The aforementioned discussion accentuates the criticality and practicality of employing decomposition methods in such analytical contexts." "The decomposition methodologies present distinct advantages for elucidating the dynamics of Lagrangian*

Residual Velocity (LRV) within generally or weakly nonlinear systems. This significance stems from the absence of comprehensive analytical solutions and definitive governing equations for LRV in generally nonlinear contexts, coupled with the constraints of analytical solutions in weakly nonlinear frameworks (Jiang and Feng, 2014; Cui et al., 2019; Chen et al., 2020). In scenarios where the Coriolis force is negligible, the Lagrangian mean momentum equations remain applicable for primary momentum balance analysis. However, these equations are inadequate for the detailed dissection of each LRV component. Notably, in circumstances where the Coriolis effect is minimally impactful, the methodologies employed for LRV decomposition may demonstrate variability, contingent upon the dominant momentum balances. This underscores the necessity for expanded investigation in future scholarly endeavors."

2. The decomposition of eddy viscosity component (i.e. section 2.1)

How do you decompose the velocity and eddy viscosity into tidal average and tidal oscillation parts? Is the tidal average Eulerian or Lagrangian average? If it is Eulerian average, what is the physical meaning of the decomposed terms? If it is Lagrangian average, terms 2 and 3 on the right hand side of Eqs. 1 and 2 should be zero.

Response: The velocity and eddy viscosity have been decomposed into tidal averages and tidal oscillations utilizing the Eulerian mean method, for the following reasons:

Firstly, it is important to emphasize that the Eulerian mean method and the Lagrangian mean method are two mathematical approaches, both of which are inherently valid. However, they yield different types of residual currents—Eulerian residual currents and Lagrangian residual currents. To be considered as representations

of residual flow fields, these currents must adhere to the characteristics of the flow field. As Lamb (1975) has indicated, any flow field must satisfy the principle of conservation of material surfaces. Eulerian residual currents do not adhere to the conservation of material surfaces, whereas Lagrangian residual currents do, which are suitable for describing long-term material transport.

Secondly, the momentum equation used in this study for physical oceanography is expressed in the Eulerian framework. The physical variables are obtained at each fixed location in the study domain. Initially described by Simpson et al. (1990), the process of tidal straining induces periodic stratification (SIPS), where tidal straining in the density field renders water columns unstable during flood tides and vice versa during ebb tides. This leads to enhanced small-scale turbulence and increased vertical mixing during flood tides, while vertical mixing is suppressed during ebb tides. Jay and Musiak (1994) demonstrated that this asymmetric mixing during the tidal cycle is the primary mechanism for generating residual currents. It is worth noting that the asymmetry in tidal mixing, as defined, is considered for each spatial point and is defined within the Eulerian framework. Therefore, in this study, we initially employed the Eulerian averaging method to obtain the four subcomponents of eddy viscosity components, which all meet momentum balance at each time and at each spatial point.

Thirdly, when investigating the dynamics of tidal straining-induced residual currents, earlier studies primarily applied Eulerian averaging method to all momentum terms, including tidal straining, in the momentum equation, resulting in the derivation of tidal straining-induced Eulerian residual circulation (e.g., Burchard et al., 2011), later

referred to as asymmetric turbulent mixing (ATM)-induced exchange flow (e.g., Cheng et al., 2011, 2013), and subsequently termed eddy viscosity–shear covariance (ESCO) flow (Dijkstra et al., 2017). In contrast, tidal straining-induced Lagrangian residual currents have not been extensively explored in previous research. Therefore, in this study, we applied Lagrangian averaging to all momentum terms, including tidal straining, in the momentum equation. The physical interpretation of this approach is that it considers the integrated effect of tidal straining at each point along the trajectory of particle motion.

Finally, when employing the Lagrangian averaging method to separate velocity and eddy viscosity into tidal averages and tidal oscillations, defining tidal asymmetry during flood and ebb tides poses a challenge. This is because particles pass through different spatial points at various times along their trajectory, rendering it challenging to establish a consistent concept of asymmetric tidal mixing that corresponds to previous definitions.

The tidal straining is represented by the ESCO, i.e. the eddy viscosity-shear covariance that is the tidal average of the product of tidal oscillations of velocity and eddy viscosity. Hence, tidal straining term is the fourth term rather than the second term in Eqs. 1 and 2.

Response: In the current manuscript, we express the horizontal velocities u and v as the sum of two components: $u=u_0+u_1$ and $v=v_0+v_1$, namely u_0 and v_0 representing the tidal periodic oscillation currents, "*which are referred to as the zero-order terms. These zero-order terms are equivalent in meaning to u' and v' as defined in prior studies (Burchard*

and Hetland, 2010; Burchard et al., 2011, 2014; Cheng, 2014). The terms u_1 and v_1 correspond to the first-order terms and represent the tidal average current" (lines 211–214). Similarly, the eddy viscosity coefficient v_h ($v_h = v_{h0} + v_{h1}$) is decomposed into v_{h0}, representing the tidal average eddy viscosity *"as the zero-order term"*, and *"v_{h1}, representing the tidal periodic oscillation of the eddy viscosity as the first-order term"*(lines 214–216). Therefore, the third term in Eqs. (1) and (2) corresponds to the tidal straining circulation.

$$-\left\langle \frac{1}{D^2}\frac{\partial}{\partial\sigma}\left(v_h\frac{\partial u}{\partial\sigma}\right)\right\rangle/f = \underbrace{-\left\langle \frac{1}{D^2}\frac{\partial}{\partial\sigma}\left(v_{h0}\frac{\partial u_0}{\partial\sigma}\right)\right\rangle/f}_{1}\underbrace{-\left\langle \frac{1}{D^2}\frac{\partial}{\partial\sigma}\left(v_{h0}\frac{\partial u_1}{\partial\sigma}\right)\right\rangle/f}_{2}$$
$$\underbrace{-\left\langle \frac{1}{D^2}\frac{\partial}{\partial\sigma}\left(v_{h1}\frac{\partial u_0}{\partial\sigma}\right)\right\rangle/f}_{3}\underbrace{-\left\langle \frac{1}{D^2}\frac{\partial}{\partial\sigma}\left(v_{h1}\frac{\partial u_1}{\partial\sigma}\right)\right\rangle/f}_{4}, \quad (1)$$

$$\left\langle \frac{1}{D^2}\frac{\partial}{\partial\sigma}\left(v_h\frac{\partial v}{\partial\sigma}\right)\right\rangle/f = \underbrace{\left\langle \frac{1}{D^2}\frac{\partial}{\partial\sigma}\left(v_{h0}\frac{\partial v_0}{\partial\sigma}\right)\right\rangle/f}_{1} + \underbrace{\left\langle \frac{1}{D^2}\frac{\partial}{\partial\sigma}\left(v_{h0}\frac{\partial v_1}{\partial\sigma}\right)\right\rangle/f}_{2} +$$
$$\underbrace{\left\langle \frac{1}{D^2}\frac{\partial}{\partial\sigma}\left(v_{h1}\frac{\partial v_0}{\partial\sigma}\right)\right\rangle/f}_{3} + \underbrace{\left\langle \frac{1}{D^2}\frac{\partial}{\partial\sigma}\left(v_{h1}\frac{\partial v_1}{\partial\sigma}\right)\right\rangle/f}_{4}, \quad (2)$$

The detailed information (lines 226–232 in the revised manuscript) is as follows: "*The $-\langle\frac{1}{D^2}\frac{\partial}{\partial\sigma}\left(v_{h0}\frac{\partial u_0}{\partial\sigma}\right)\rangle/f$ and $\langle\frac{1}{D^2}\frac{\partial}{\partial\sigma}\left(v_{h0}\frac{\partial v_0}{\partial\sigma}\right)\rangle/f$ represent the coupled component of the tidal-average eddy viscosity and velocity gradient oscillation (v_{Lk0u0} and u_{Lk0u0}), **the $-\langle\frac{1}{D^2}\frac{\partial}{\partial\sigma}\left(v_{h1}\frac{\partial u_0}{\partial\sigma}\right)\rangle/f$ and $\langle\frac{1}{D^2}\frac{\partial}{\partial\sigma}\left(v_{h1}\frac{\partial v_0}{\partial\sigma}\right)\rangle/f$ represent the tidal straining component (v_{Lk1u0} and u_{Lk1u0}),** the $-\langle\frac{1}{D^2}\frac{\partial}{\partial\sigma}\left(v_{h0}\frac{\partial u_1}{\partial\sigma}\right)\rangle/f$ and $\langle\frac{1}{D^2}\frac{\partial}{\partial\sigma}\left(v_{h0}\frac{\partial v_1}{\partial\sigma}\right)\rangle/f$ represent the turbulent mean component (v_{Lk0u1} and u_{Lk0u1}), the $-\langle\frac{1}{D^2}\frac{\partial}{\partial\sigma}\left(v_{h1}\frac{\partial u_1}{\partial\sigma}\right)\rangle/f$ and $\langle\frac{1}{D^2}\frac{\partial}{\partial\sigma}\left(v_{h1}\frac{\partial v_1}{\partial\sigma}\right)\rangle/f$ represent the coupled component of eddy viscosity oscillation and the tidal-average velocity gradient (v_{Lk1u1} and u_{Lk1u1}).*" The $-\langle\frac{1}{D^2}\frac{\partial}{\partial\sigma}\left(v_{h1}\frac{\partial u_0}{\partial\sigma}\right)\rangle/f$ and $\langle\frac{1}{D^2}\frac{\partial}{\partial\sigma}\left(v_{h1}\frac{\partial v_0}{\partial\sigma}\right)\rangle/f$ represent the tidal straining

components of the LRV, corresponding to the third term in Eqs. (1) and (2). These components reflect the covariance between the oscillation of eddy viscosity and velocity shear, arising specifically due to the fact that v_{h1}, u_0, and v_0 are all oscillatory terms.

The total water depth, D also changes with time, and needs to be decomposed in the same way as the velocity and eddy viscosity do.

Response: Applying a first-order Taylor expansion, the approximation of $1/D^2$ can be expressed as $1/H^2 - 2\zeta/H^3$ (Cheng, 2014), where H represents the mean depth, ζ denotes sea surface elevation. The four subcomponents of the eddy viscosity component, as delineated in Eqs. (1) and (2) in the revised manuscript, are further decomposed into eight distinct terms, detailed in Eqs. (A3) and (A4).

$$
\begin{aligned}
-\left\langle \frac{1}{D^2}\frac{\partial}{\partial\sigma}\left(v_h\frac{\partial u}{\partial\sigma}\right)\right\rangle/f = {} & \underbrace{-\left\langle \frac{1}{H^2}\frac{\partial}{\partial\sigma}\left(v_{h0}\frac{\partial u_0}{\partial\sigma}\right)\right\rangle/f}_{1} \underbrace{-\left\langle \frac{1}{H^2}\frac{\partial}{\partial\sigma}\left(v_{h0}\frac{\partial u_1}{\partial\sigma}\right)\right\rangle/f}_{2} \\
& \underbrace{-\left\langle \frac{1}{H^2}\frac{\partial}{\partial\sigma}\left(v_{h1}\frac{\partial u_0}{\partial\sigma}\right)\right\rangle/f}_{3} \underbrace{-\left\langle \frac{1}{H^2}\frac{\partial}{\partial\sigma}\left(v_{h1}\frac{\partial u_1}{\partial\sigma}\right)\right\rangle/f}_{4} \\
& \underbrace{-\left\langle \frac{-2\zeta}{H^3}\frac{\partial}{\partial\sigma}\left(v_{h0}\frac{\partial u_0}{\partial\sigma}\right)\right\rangle/f}_{5} \underbrace{-\left\langle \frac{-2\zeta}{H^3}\frac{\partial}{\partial\sigma}\left(v_{h0}\frac{\partial u_1}{\partial\sigma}\right)\right\rangle/f}_{6} \\
& \underbrace{-\left\langle \frac{-2\zeta}{H^3}\frac{\partial}{\partial\sigma}\left(v_{h1}\frac{\partial u_0}{\partial\sigma}\right)\right\rangle/f}_{7} \underbrace{-\left\langle \frac{-2\zeta}{H^3}\frac{\partial}{\partial\sigma}\left(v_{h1}\frac{\partial u_1}{\partial\sigma}\right)\right\rangle/f}_{8},
\end{aligned}
\tag{A3}
$$

$$
\begin{aligned}
\left\langle \frac{1}{D^2}\frac{\partial}{\partial\sigma}\left(v_h\frac{\partial v}{\partial\sigma}\right)\right\rangle/f = {} & \underbrace{\left\langle \frac{1}{H^2}\frac{\partial}{\partial\sigma}\left(v_{h0}\frac{\partial v_0}{\partial\sigma}\right)\right\rangle/f}_{1} + \underbrace{\left\langle \frac{1}{H^2}\frac{\partial}{\partial\sigma}\left(v_{h0}\frac{\partial v_1}{\partial\sigma}\right)\right\rangle/f}_{2} + \\
& \underbrace{\left\langle \frac{1}{H^2}\frac{\partial}{\partial\sigma}\left(v_{h1}\frac{\partial v_0}{\partial\sigma}\right)\right\rangle/f}_{3} + \underbrace{\left\langle \frac{1}{H^2}\frac{\partial}{\partial\sigma}\left(v_{h1}\frac{\partial v_1}{\partial\sigma}\right)\right\rangle/f}_{4} + \\
& \underbrace{\left\langle \frac{-2\zeta}{H^3}\frac{\partial}{\partial\sigma}\left(v_{h0}\frac{\partial v_0}{\partial\sigma}\right)\right\rangle/f}_{5} + \underbrace{\left\langle \frac{-2\zeta}{H^3}\frac{\partial}{\partial\sigma}\left(v_{h0}\frac{\partial v_1}{\partial\sigma}\right)\right\rangle/f}_{6} +
\end{aligned}
\tag{A4}
$$

$$\underbrace{\left\langle \frac{-2\zeta}{H^3}\frac{\partial}{\partial\sigma}\left(v_{h1}\frac{\partial v_0}{\partial\sigma}\right)\right\rangle/f}_{7}+\underbrace{\left\langle \frac{-2\zeta}{H^3}\frac{\partial}{\partial\sigma}\left(v_{h1}\frac{\partial v_1}{\partial\sigma}\right)\right\rangle/f}_{8},$$

In the majority of the Pearl River Estuary, the ratio of maximum sea surface elevation (ζ_{max}) to mean water depth (H) is less than 0.2 during neap tides, except in the nearshore areas. The terms related to $-2\zeta/H^3$, including the fifth to eighth terms in Eqs. (A3) and (A4), are so minimal that they can be considered negligible during neap tides (Fig. A2a3–j3). Conversely, the terms related to $1/H^2$, comprising the first to fourth terms (Fig. A2a2–j2) in Eqs. (A3) and (A4), demonstrate a notable congruence with the terms related to$1/D^2$ in structure and magnitude during neap tides (Fig. A2a1–j1). During spring tides, although the ratio of ζ_{max} to H is slightly larger than those during neap tides, the terms associated with $1/H^2$ (Fig. A3a2–j2) continue to predominate in both structure and magnitude over the components related to $1/D^2$ (Fig. A3a1–j1). Additionally, while the terms associated with $-2\zeta/H^3$ (Fig. A3a3–j3) are greater during spring tides than during neap tides, their contribution to the total components remains significantly less than those related to $1/H^2$. Given that D is approximately equal to H, D is not decomposed further in the manuscript. The relevant content has already been included in the text. "*Employing a first-order Taylor expansion, the approximation of* $1/D^2$ *is represented as* $1/H^2–2\zeta/H^3$ *(Cheng, 2014), where H signifies the mean depth and* ζ *corresponds to the sea surface elevation. Within the vast majority of the Pearl River Estuary, the ratio of* ζ_{max} *to H remains below 0.2 during neap tides, with an exception in nearshore areas, where* ζ_{max} *is the maximum of tidal elevations during a tidal period. The ratio during spring tides is slightly bigger than that during neap tides.*

But whether during spring or neap tides, the terms associated with $1/H^2$ exhibit a close correspondence to those related to $1/D^2$ in Eqs. (1) and (2) (not shown). The terms pertaining to $-2\zeta/H^3$ are sufficiently minor to be negligible. Consequently, considering D is approximately equivalent to H, further decomposition of D in the manuscript is not undertaken." (lines 217–226)

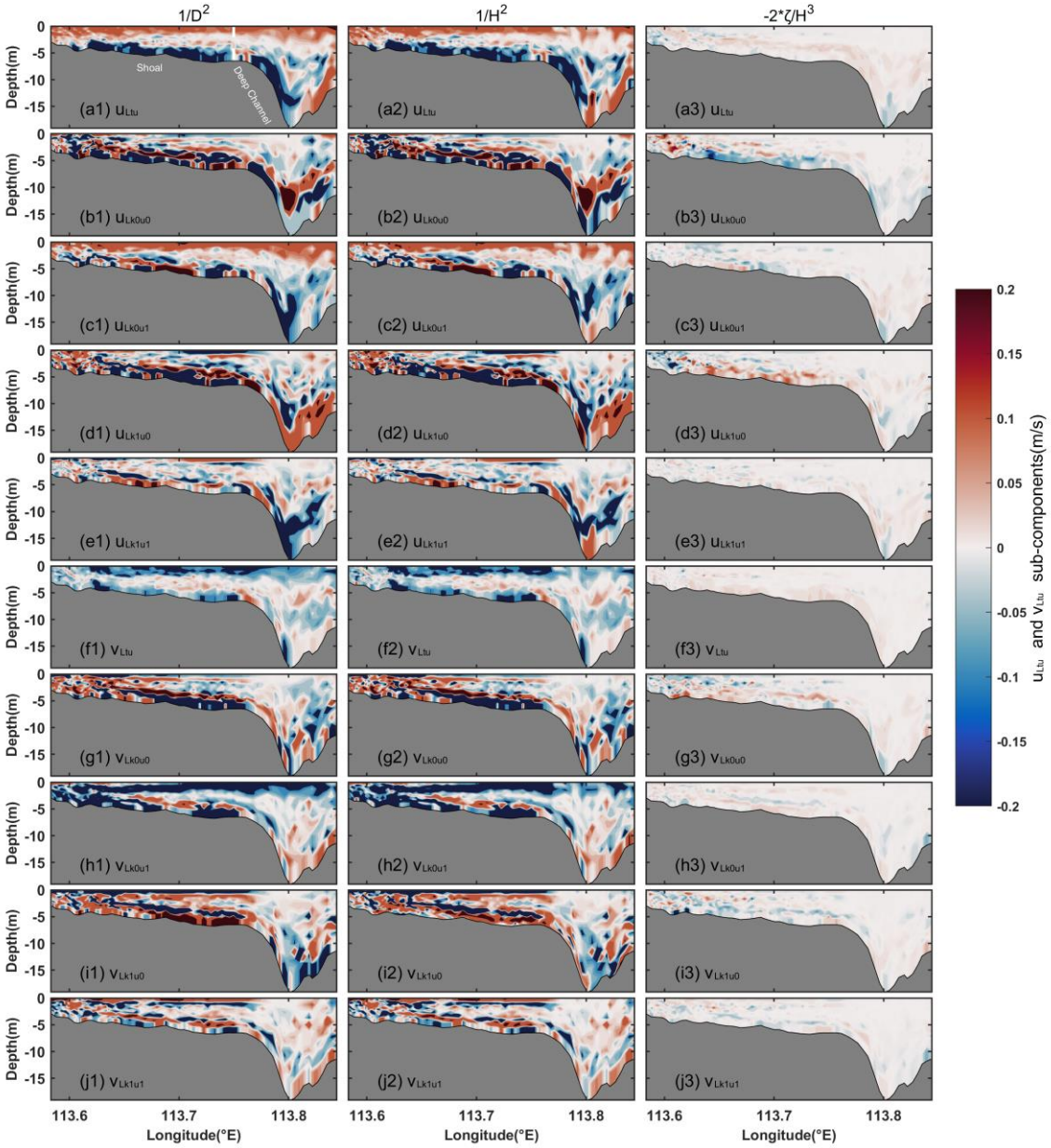

Figure A2 Vertical profiles of each subcomponent of the eddy viscosity during neap tides. **(a1–j1)** terms related to $1/D^2$, **(a2–j2)** terms related to $1/H^2$, **(a3–j3)** terms related to $-2\zeta/H^3$. For cross-estuary direction:

(a1, a2, a3) total eddy viscosity component related to 1/ D^2, 1/H^2 and –2ζ/H^3, respectively; **(b1, b2, b3)** coupled component of the tidal-average eddy viscosity and velocity gradient oscillation (u_{Lk0u0}) related to1/D^2, 1/H^2 and –2ζ/H^3; **(c1, c2, c3)** turbulent mean component (u_{Lk0u1}) related to 1/D^2, 1/H^2 and –2ζ/H^3, **(d1, d2, d3)** tidal straining component (u_{Lk1u0}) related to 1/D^2, 1/H^2 and –2ζ/H^3; **(e1, e2, e3)** coupled component of eddy viscosity oscillation and the tidal-average velocity gradient (u_{Lk1u1}) related to 1/D^2, 1/H^2 and –2ζ/H^3, respectively. **(f1–j1; f2–j2; f3–j3)** Corresponding along-estuary subcomponents related to 1/D^2, 1/H^2 and –2ζ/H^3.

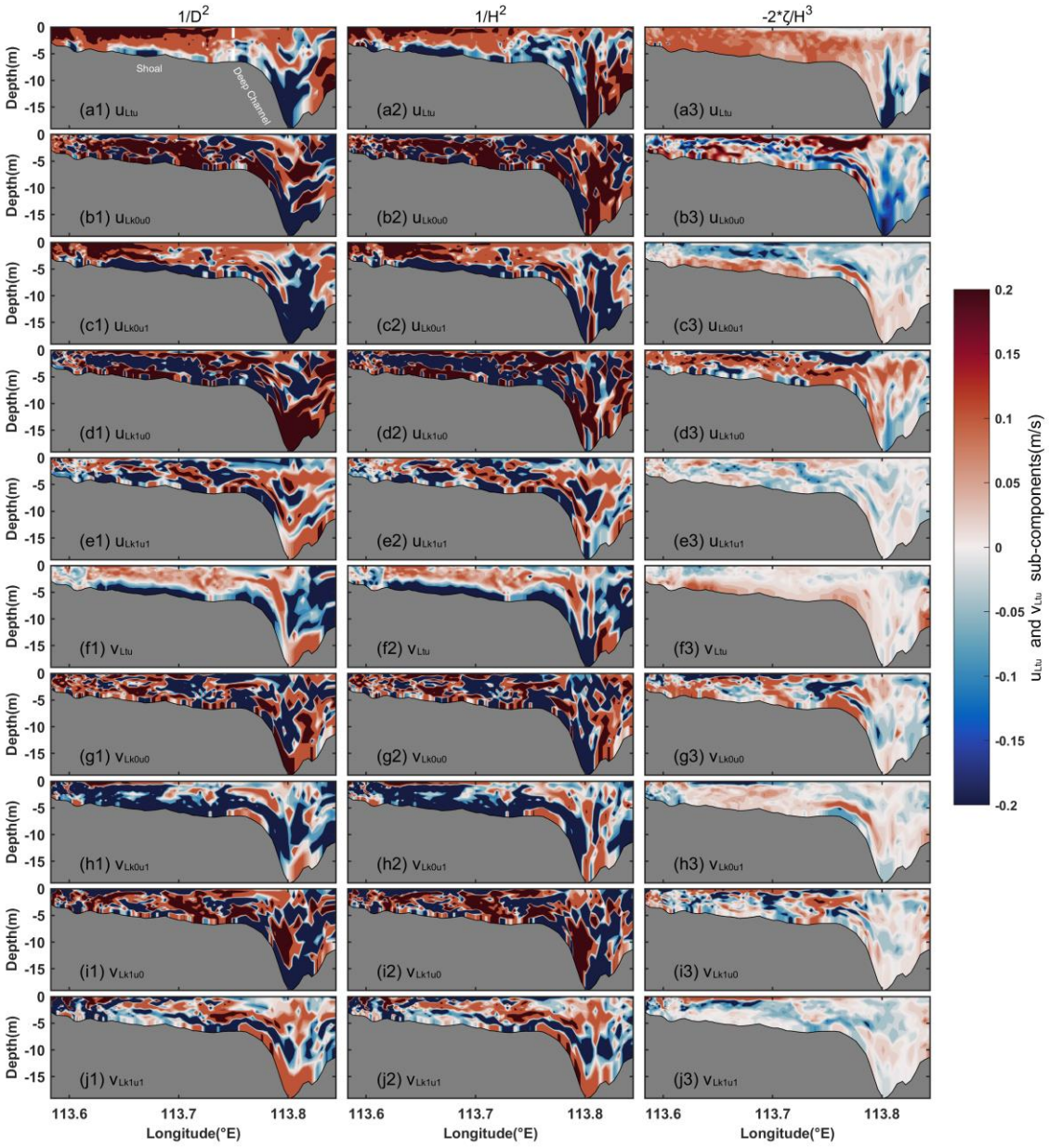

Figure A3 Same as Fig. A2, but for spring tides.

Fig. 4 b, line 280-282. Why does the barotropic component have a vertical two-layer structure?

Response: To elucidate the two-layer structure of the barotropic component of LRV as depicted in Fig. A4a, we conducted an integration of the barotropic pressure gradient forcing (BPG) along the particle's trajectory throughout a tidal cycle, denominated as Lagrangian integrated BPG. This methodology encompasses the cumulative effects at each point traversed by the particle. Distinct trajectories undertaken by surface and bottom particles result in divergent outcomes with different magnitudes and opposing signs for the Lagrangian integrated BPG across the upper and lower layers, as illustrated in Fig. A4b–c. The Lagrangian integrated BPG at the final step, divided by one tidal period, yields the Lagrangian mean BPG. Consequently, the corresponding Lagrangian residual velocity is characterized by a vertically sheared two-layer structure with opposite flow directions. Contrastingly, the Eulerian mean BPG, averaged at fixed spatial points, exhibits a homogeneous vertical profile (Fig. A5a). Notably, discrepancies are also observed between Lagrangian integrated and Eulerian mean baroclinic pressure gradient forcings, expounded upon in Fig. A4d–f and Fig. A5b. The related explanation has been added in the manuscript (lines 341–344). "*The two-layer structure of* u_{Lba} *arises from the distinct trajectories of particles in the upper and lower layers. The integration results along these different trajectories produce varying magnitudes and opposite directions of* u_{Lba} *components in both layers.*"

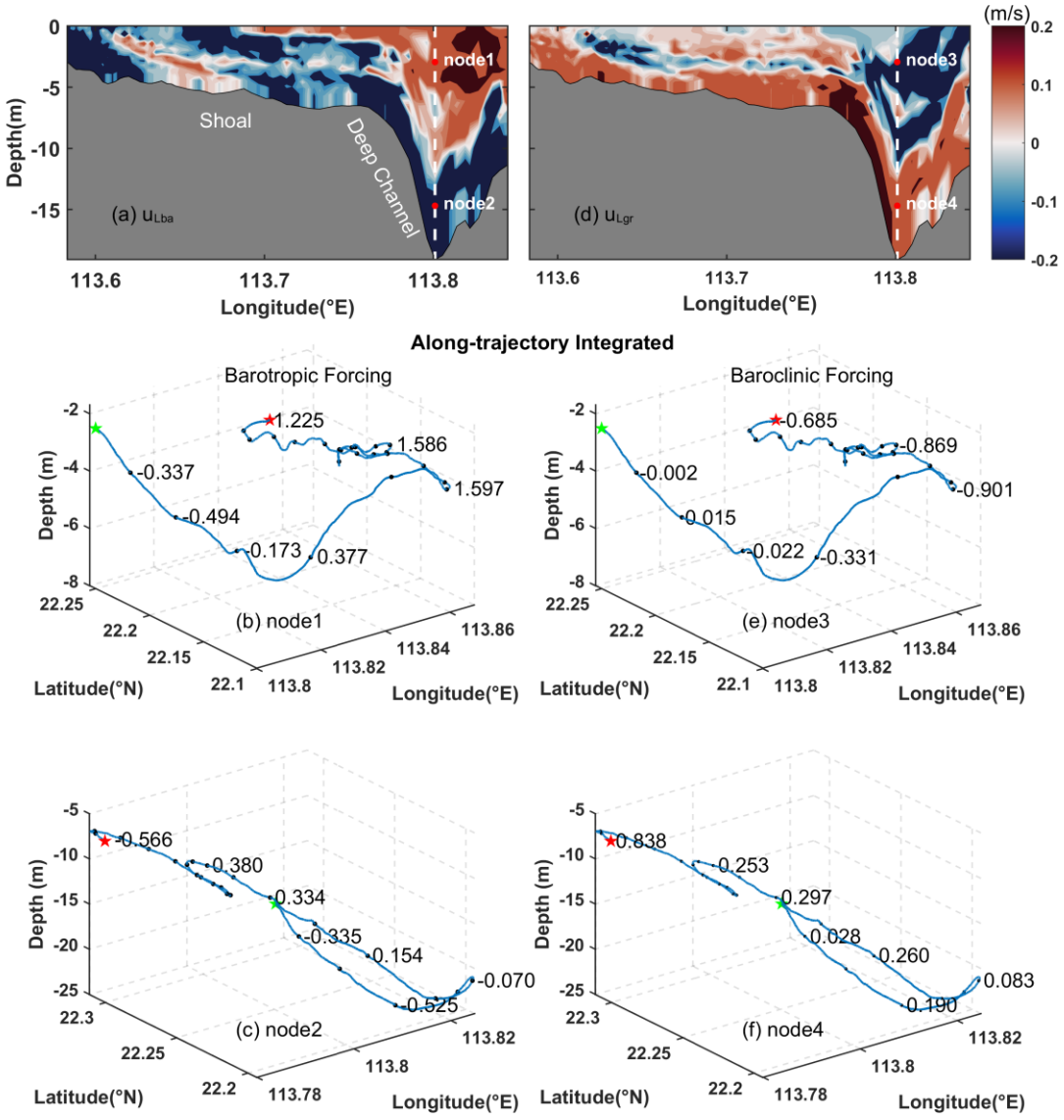

Figure A4 (a) The cross-estuary barotropic component of the Lagrangian Residual Velocity (LRV), with two red nodes (nodes 1 and 2) in the deep channel indicating locations of eastward and westward flow, respectively. **(b, c)** Lagrangian-integrated barotropic pressure gradient along the trajectories of particles at nodes 1 and 2, respectively. The green star marks the starting location, while the red star denotes the ending location. The particle trajectories are traced with blue lines. **(d–f)** Same as **(a–c)**, but for the baroclinic component of LRV at nodes 3 and 4, respectively.

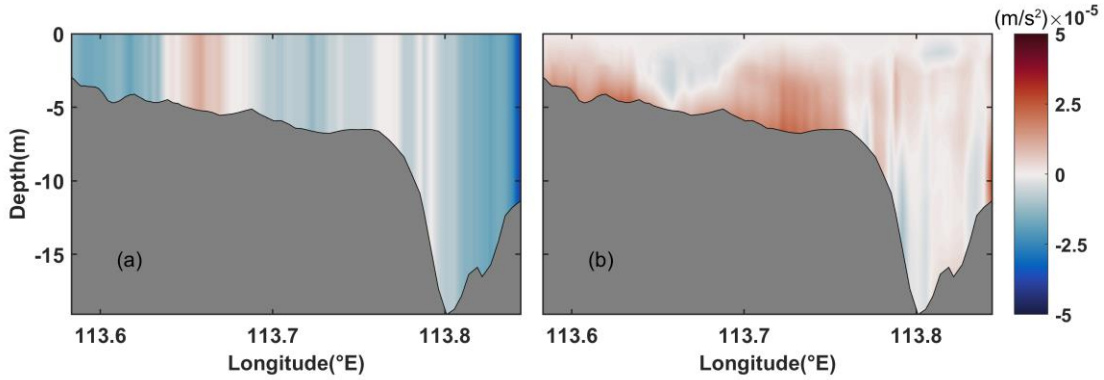

Figure A5 Vertical profiles of the Eulerian mean **(a)** barotropic and **(b)** baroclinic pressure gradient forcing in Section C.

Reference

Burchard, H., Hetland, R. D.: Quantifying the contributions of tidal straining and gravitational circulation to residual circulation in periodically stratified tidal estuaries, J. Phys. Oceanogr., 40(6), 1243–1262, https://doi.org/10.1175/2010JPO4270.1, 2010.

Burchard, H., Hetland, R. D., Schulz, E., Schuttelaars, H. M.: Drivers of residual estuarine circulation in tidally energetic estuaries: Straight and irrotational channels with parabolic cross section, J. Phys. Oceanogr., 41(3), 548–570, https://doi.org/10.1175/2010JPO4453.1, 2011.

Burchard, H., Schulz, E., Schuttelaars, H. M.: Impact of estuarine convergence on residual circulation in tidally energetic estuaries and inlets, Geophys. Res. Lett., 41(3), 913–919, https://doi. org/10.1002/2013GL058494, 2014.

Chen, Y., Cui, Y. X., Sheng, X. X., Jiang, W. S., Feng, S. Z.: Analytical solution to the 3D tide-induced Lagrangian residual current in a narrow bay with vertically varying eddy viscosity coefficient, Ocean Dyn., 70, 759–770, https://doi.org/10.1007/s10236-020-01359-3, 2020.

Chen, Y. R., Chen, L. H., Zhang, H., Gong, W. P.: Effects of wave-current interaction on the Pearl River Estuary during Typhoon Hato, Estuar. Coast. Shelf Sci., 228, 106364, https://doi.org/10.1016/j.ecss.2019.106364, 2019.

Cheng, P.: Decomposition of residual circulation in estuaries, J. Atmos. Ocean. Tech., 31(3), 698–713, 2014.

Cheng, P., de Swart H. E., Valle-Levinson, A.: Role of asymmetric tidal mixing in the subtidal dynamics of narrow estuaries, J. Geophys. Res.: Oceans, 118(5), 2623–2639, https://doi.org/10.1002/jgrc.20189, 2013.

Cheng, P., Valle-Levinson, A., de Swart, H. E.: A numerical study of residual circulation induced by asymmetric tidal mixing in tidally dominated estuaries, J. Geophys. Res.: Oceans, 116(C1), https://doi.org/10.1029/2010JC006137, 2011.

Cui, Y. X., Jiang, W. S., Deng, F. J.: 3D numerical computation of the tidally induced Lagrangian residual current in an idealized bay, Ocean Dyn., 69, 283–300, https://doi.org/10.1007/s10236-018-01243-1, 2019.

Dijkstra, Y. M., Schuttelaars, H. M., Burchard, H.: Generation of exchange flows in estuaries by tidal and gravitational eddy viscosity-shear covariance (ESCO), J. Geophys. Res.: Oceans, 122(5), 4217–4237, https://doi.org/10.1002/2016JC012379, 2017.

Jay, D. A., Musiak, J. D.: Particle trapping in estuarine tidal flows, J. Geophys. Res.: Oceans, 99(C10), 20445–20461, https://doi.org/10.1029/94JC00971, 1994.

Jiang, W. S., Feng, S. Z.: Analytical solution for the tidally induced Lagrangian residual current in a narrow bay, Ocean Dyn., 61, 543–558, https://doi.org/10.1007/s10236-011-0381-z, 2011.

Jiang, W. S., Feng, S. Z.: 3D analytical solution to the tidally induced Lagrangian residual current equations in a narrow bay, Ocean Dyn., 64, 1073–1091, https://doi.org/10.1007/s10236-014-0738-1, 2014.

Lai, W. F., Pan, J. Y., Devlin, A. T.: Impact of tides and winds on estuarine circulation in the Pearl River Estuary, Cont. Shelf Res., 168, 68–82, https://doi.org/10.1016/j.csr.2018.09.004, 2018.

Lamb, H.: Hydrodynamics, London: Cambridge university press, 1975.

Li, M. Q., Wang, N., Li, G. X., Song, D. H., Gu, Y. Z., Bao, X. W., Liu, S. D., Zhang, L.: Plume bulge observed in the Pearl River Estuary in summer: Spatiotemporal characteristics and influencing factors, Estuar. Coast. Shelf Sci., 282, 108242, 2023.

Pan, J. Y., Gu, Y. Z., Wang, D. X.: Observations and numerical modeling of the Pearl River plume in summer season, J. Geophys. Res.: Oceans, 119(4), 2480–2500, 2014.

Simpson, J. H., Brown, J., Matthews, J., Allen, G.: Tidal straining, density currents, and stirring in the control of estuarine stratification, Estuaries 13, 125–132, https://doi.org/10.2307/1351581, 1990.

Wu, H., Gu, J. H., Zhu, P.: Winter counter-wind transport in the inner southwestern Yellow Sea, J. Geophys. Res.: Oceans, 123(1), 411–436, 2018.